FERMILAB-CONF-06-306-AD

PHOTOINJECTOR PRODUCTION OF A FLAT BEAM WITH TRANSVERSE EMITTANCE RATIO OF 100*

P. Piot, Northern Illinois University DeKalb, IL 60115, & Fermilab, Batavia, IL 60510, USA
Y.-E Sun †, University of Chicago, Chicago, IL 60637, USA
K.-J. Kim, Argonne National Laboratory, Argonne, IL 60439, USA

Abstract

The generation of a flat electron beam directly from a photoinjector is an attractive alternative to the electron damping ring as envisioned for linear colliders. It also has potential applications to light sources such as the generation of ultrashort x-ray pulses or Smith-Purcell free electron lasers. In this paper, we report on the experimental generation of a flat beam with a measured transverse emittance ratio of 100 ± 20 for a bunch charge of $\simeq 0.5$ nC. The experimental data, obtained at the Fermilab/NICADD Photoinjector Laboratory, are compared with numerical simulations and the expected scaling laws. Possible improvement of the experiment along with application for such a flat beams are discussed.

INTRODUCTION

In this paper, the latest results on the flat-beam production experiment at Fermilab/NICADD photoinjector (FNPL) [1] are presented; more details can be found in Ref. [2]. Since the proof-of-principle experiment reported in Ref. [3], the experimental setup has been improved and systematic studies were conducted [4, 5, 6]. At FNPL, electron bunches are produced in a 1.3 GHz radiofrequency (rf) photoemission electron source, and accelerated to 16 MeV in a TESLA-type superconducting cavity. Downstream of the accelerating cavity, three skew quadrupoles can be used to produce a flat beam when the incoming beam is angular-momentum dominated [7, 8, 9]. The nominal operating parameters of FNPL are given in Table 1. The rf-gun and booster-cavity settings are kept the same during the experiment whereas the drive-laser spot size on the photocathode and the solenoid currents are adjusted for the different sets of measurements reported hereafter.

Upon proper tuning of the transformer, the expected normalized flat-beam emittances, $\varepsilon_n^{\pm}$, are given by [9]

$$\varepsilon_n^{\pm} = \sqrt{(\varepsilon_n^u)^2 + (\beta\gamma\mathcal{L})^2} \pm (\beta\gamma\mathcal{L}) \xrightarrow{\beta\gamma\mathcal{L} \gg \varepsilon_n^u} \begin{cases} \varepsilon_n^+ \simeq 2\beta\gamma\mathcal{L} \\ \varepsilon_n^- \simeq \frac{(\varepsilon_n^u)^2}{2\beta\gamma\mathcal{L}} \end{cases}, \quad (1)$$

where $\varepsilon_n^u = \beta\gamma\varepsilon_u$ is the normalized uncorrelated emittance of the magnetized beam prior to the transformer, $\beta = v/c$, γ is the Lorentz factor, $\mathcal{L} = \langle L \rangle / 2p_z$, p_z is the longitudinal momentum, and $\langle L \rangle \equiv eB_0\sigma_c^2$, where e is the electron charge, B_0 the axial magnetic field on the photocathode surface, and σ_c the root-mean-square (rms) transverse size of the drive-laser spot on the photocathode

Table 1: Nominal settings for the photocathode drive laser, rf gun and accelerating section during the flat-beam experiment.

parameter	value	unit
laser injection phase	25	degree
rms laser light size on cathode	$0.75 \sim 1$	mm
laser pulse duration (Gaussian)	3 or 6	ps
bunch charge	0.5	nC
E_z on cathode	32	MV/m
B_0 on cathode	$400 \sim 900$	Gauss
booster cavity peak gradient	23	MV/m

EXPERIMENT & SIMULATION

Quadrupole Settings

Given the initial experimental conditions, numerical simulation are performed with the program ASTRA [10] and the initial skew quadrupole settings needed to transform the magnetized round beam in a flat beam are determined from these numerical simulations together with a simplex minimization algorithm. The devised skew quadrupole strengths are used as initial values in the experiment and are then empirically fine-tuned to insure the x-y correlation on the beam has been removed downstream of the RFTB. This is done by inspecting the beam transverse density on X7 and X8: upon removal of the angular momentum, the beam should remain flat and upright on all the viewers downstream of the RFTB. In Table 2 we compare, for two cases of rms drive-laser spot sizes (σ_c=0.76 mm and σ_c =0.97 mm), the final quadrupole currents used in the experiment with the initial values obtained numerically. Most of the quadrupole currents agree with predicted values, the larger discrepancies observed for the settings of the last quadrupole reflect a looser tolerance on this quadrupole setting [4].

* Work supported by Universities Research Association Inc. under Contract No. DEAC02- 76CH00300 with the U.S. Department of Energy and by the Northern Illinois Center of Accelerator and Detector Development (NICADD).

† Now at Argonne National Laboratory

Table 2: Comparison of the skew quadrupole currents used in experiment with the one predicted from simulation for two case of initial conditions. Case 1: $\sigma_c = 0.79$ mm, Case 2: $\sigma_c = 0.97$ mm. I_i represents the current of the skew quadrupole used in the round-to-flat beam transformer.

quadrupole	case 1		case 2	
current	exp.	sim.	exp.	sim.
I_1(A)	-1.92	-2.03	-1.97	-1.98
I_2(A)	2.40	2.57	2.56	2.58
I_3(A)	-2.99	-4.01	-4.55	-5.08

Best Flat Beam Emittance Ratio

For the transverse emittance measurements, the beam images on the different viewers are taken for a single-bunch beam. In Figure 1, we present the set of experimental images, along with their respective simulated images, needed to infer the two transverse flat-beam emittances. In Table 3, we gather the measured and simulated parameters for the case of $\sigma_c = 0.97$ mm. The smaller of the normalized flat beam emittance is $\varepsilon_n^x = 0.41 \pm 0.06$ μm; this is less than half of the expected thermal emittance due to the photoemission process of the cesium telluride material. From [11, 12], we infer the thermal emittance to be $\varepsilon_{th} = 0.99 \pm 0.10$ μm given $\sigma_c = 0.97 \pm 0.05$ mm.

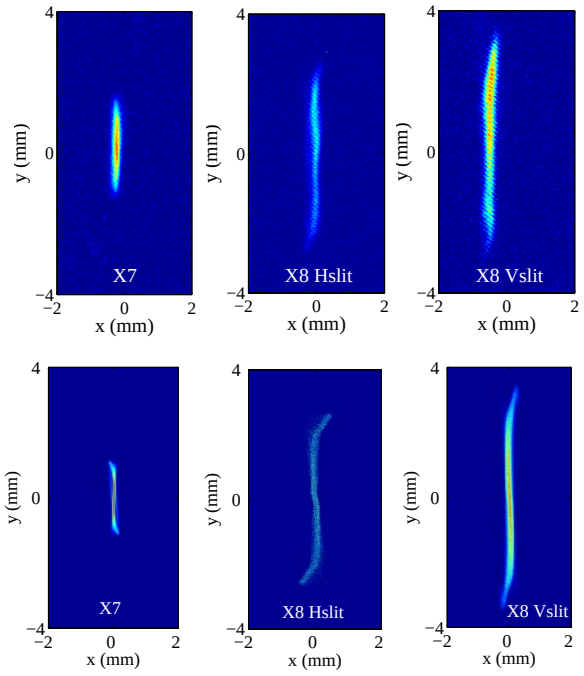

Figure 1: Top three images are taken with digital cameras: beam at X7, horizontal and vertical slit images at X8. Bottom three are the corresponding beam profiles from ASTRA simulations. These images are associated with the flat-beam presented in Table 3.

Table 3: Measured and simulated flat-beam parameters for $\sigma_c = 0.97$ mm. Both systematic and statistical (in brackets) errorbars are included.

parameter	experiment	simulation	unit
σ_x^{X7}	0.088±0.01 (±0.01)	0.058	mm
σ_y^{X7}	0.63±0.01 (±0.01)	0.77	mm
$\sigma_x^{X8,v}$	0.12±0.01 (±0.01)	0.11	mm
$\sigma_y^{X8,h}$	1.68±0.09 (±0.01)	1.50	mm
ε_n^x	0.41±0.06 (±0.02)	0.27	μm
ε_n^y	41.1±2.5 (±0.54)	53	μm
$\varepsilon_n^y/\varepsilon_n^x$	100.2±20.2 (±5.2)	196	–

Transverse Emittance Partitioning

To gain more insight into the round-to-flat-beam transformation, we compare the expected flat-beam emittances, $\varepsilon_n^{\pm}$ in Eq. (1), given the incoming magnetized beam parameters, with the measured flat-beam emittances downstream of the transformer. The uncorrelated emittance of the magnetized beam ε_n^u is measured using the slit technique from the beam image at X3 and the corresponding slit images at X5. $\mathcal{L}$ has been obtained with the two different methods detailed in [5]. The resulting measurements for the case $\sigma_c = 0.97$ mm are summarized in Table 4: within the experimental errors we observed that the measured four-dimensional (4-D) emittance $\varepsilon_{4D} \equiv \sqrt{\varepsilon_n^x \varepsilon_n^y}$ is conserved during the round-to-flat-beam transformation.

Table 4: Parameters measured from the angular-momentum-dominated round beam and the corresponding flat beam.

parameters	round-beam	flat-beam	simulation
$\beta\gamma\mathcal{L}$	25.6±2.6	–	26.3
ε_n^u	5.1±0.9	–	3.8
ε_n^+	53.8±5.4[a]	41.0±2.5	53
ε_n^-	0.49±0.22[a]	0.41±0.06	0.27
$\sqrt{\varepsilon_n^+ \varepsilon_n^-}$	5.1±0.9	4.1±0.8	3.8

[a] expected value given the measured round beam parameters.

We note a ∼25% discrepancy for the measured larger flat-beam emittance, compared to the simulation and the value predicted from the round beam parameters. This is probably due to imperfectly optimized settings for the transformer.

We finally report the dependence of ε_n^+ versus $\mathcal{L}$. The value of $\mathcal{L}$ was varied either by changing B_0 or σ_c. As expected ε_n^+ is linearly dependent on $\mathcal{L}$, and a linear regression gives $\varepsilon_n^+ = (1.78 \pm 0.26)\mathcal{L}$; see Fig. 2. The slope is in agreement with the theoretically expected slope value of 2 in the limit $\mathcal{L} \gg \beta\gamma\varepsilon_n^u$; see Eq. (1).

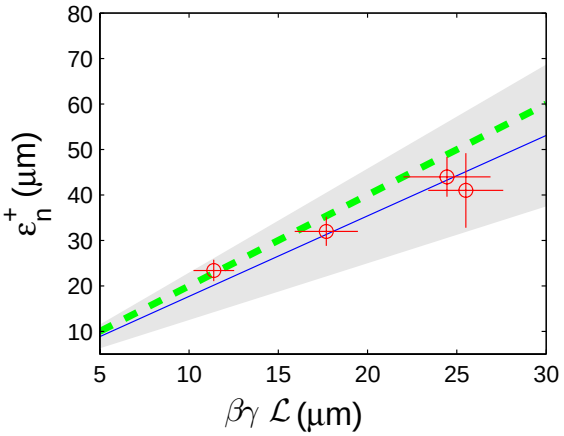

Figure 2: Larger one of the flat beam emittances (ε_n^+) versus $\beta\gamma\mathcal{L}$. A linear regression (solid line) of the experimental data (circle) is compared with the theoretical dependence (dashed line). The shaded area represents the 95% confidence bounds associated with the linear regression.

Experimental Limitations

The lower limit for the best measured emittance ratio of $\sim$100 is currently limited by our experimental set-up: the fact that the transformation occurs at low energy along with $\sigma_\delta \simeq 0.25\%$ made our measurement sensitive to spurious dispersion. Simulations based on steering dipole settings used to correct the beam orbit indicate that the thereby introduced dispersion could result in an overestimation of the smaller flat-beam emittance by a factor up to 2. Spurious dispersion accounts for most of the discrepancy between numerical simulations and measurements. The experiment is limited to low charge in order to avoid space charge to significantly impact the beam dynamics in the transformation at 16 MeV. A possible improvement, aimed at reducing spurious dispersion effects, would consist in further accelerating the beam after the flat-beam transformation such to decrease the fractional momentum spread.

POTENTIAL APPLICATIONS

The results presented in this paper support the potential flat-beam injector designs for the LUX light source proposal at Berkeley [13].

Our results also open path for Smith-Purcell-based free-electron lasers (FEL) either at low energy, where the device operate in the backward wave oscillator [14, 15], or at high energy, using a so-called image charge undulator [16]. The former configuration is envisioned as a compact tunable terahertz source. The advantage of using Smith-Purcell radiation for short-wavelength free-electron laser is the low beam energy required to reach Angstrom-wavelength (Reference [16] discusses a Smith-Pucell operating at 1 Å with a 200 MeV electron beam).

The flat beam technique discussed in this paper is also being implemented in sheet-beam klystrons [17].

Finally the production of flat electron-beam with such a high emittance ratio is attractive for the International Linear Collider, since it may circumvent the use of an electron damping ring. However the main challenge is to also achieve, for the nominal charge of $Q = 3.2$ nC, a 4-D emittance $\varepsilon_{4D} \sim 0.4$ μm along with an emittance ratio of ~ 300. The required value for the 4-D emittance is one order of magnitude lower than what present state-of-art electron sources can reliably achieve. To this end, a possible solution might be to implement the flat beam technique together with the longitudinal-to-transverse emittance exchange [18] as recently proposed to enhance the performance of high-gain free-electron lasers [19].

REFERENCES

[1] for informations see the world wide web `http://nicadd.niu.edu/fnpl`.

[2] P. Piot, Y.-E Sun, K.-J Kim, Phys. Rev. ST Accel. Beams **9**, 031001 (2006)

[3] D. Edwards *et al.*, in *Proceedings of the XX International Linac Conference, Monterey, CA*, pp. 122-124 (2000).

[4] Y.-E Sun, phD Thesis University of Chicago (2005), also report Fermilab-thesis-2005-17 (2005).

[5] Y.-E Sun, *et al.*, Phys. Rev. ST Accel. Beams **7**, 123501 (2004).

[6] Y.-E Sun, K.-J. Kim, and P. Piot, in *Proceedings of the XXII International Linac Conference, Lubeck, Germany*, pp. 150-152 (2004)

[7] Ya. Derbenev, University of Michigan Report No. UM-HE-98-04, 1998.

[8] R. Brinkmann, Y. Derbenev and K. Flöttmann, Phys. Rev. ST Accel. Beams **4**, 053501 (2001).

[9] K.-J. Kim, Phys. Rev. ST Accel. Beams **6**, 104002 (2003).

[10] K. Flöttmann, "ASTRA: A Space Charge Tracking Algorithm", available at `http://www.desy.de/~mpyflo`.

[11] V. V. Mitchev, et al., in *Proceedings of the 2004 FEL Conference*, pp. 399-402 (2004).

[12] K. Flöttmann, DESY report TESLA-FEL-1997-01, 1997 (available from DESY-Hamburg, Germany).

[13] J. Corlett, et. al., in *Proceedings of the 2003 Particle Accelerator Conference, Portland, OR*, pp. 186-188 (2003).

[14] H. L. Andrews and C. A. Brau, Phys. Rev. ST Accel. Beams **7**, 070701 (2004).

[15] V. Kumar and K.-J. Kim, Phys. Rev. **E 73**, 026501 (2006).

[16] Y. Zhang, Ya. Derbenev and R. Li, Nucl. Instrum. Methods A **507** 459-463 (2003).

[17] K. Bishofberger, private communication (July 2006).

[18] M. Cornacchia and P. Emma, Phys. Rev. ST Accel. Beams **5**, 084001 (2002).

[19] P. Emma, *et al.*, "Transverse-to-Longitudinal Emittance Exchange to Improve Performance of High-Gain Free-Electron Lasers", submitted to Phys. Rev. ST Accel. Beams, preprint FERMILAB-PUB-06-256-AD/SLAC PUB 1000-86 (2006).